JMEPEG (2011) 20:1049–1054
DOI: 10.1007/s11665-010-9720-3

1059-9495/$19.00

Research on Process and Microstructure Formation of W-Ni-Fe Alloy Fabricated by Selective Laser Melting

Danqing Zhang, Qizhou Cai, Jinhui Liu, and Ruidi Li

(Submitted December 28, 2009; in revised form May 23, 2010)

W-Ni-Fe alloys are important materials for many practical applications; however, at present, they are usually fabricated by conventional powder metallurgy techniques, which is difficult in fabrication with complex shapes. In this work, a selective laser melting (SLM) processing method was developed for fabricating W-Ni-Fe alloys parts. A process map was obtained for selection of proper laser parameters by optimizing processing conditions. Microstructures of laser fabricated samples in different laser energy inputs were investigated. There are two coexisting forming mechanisms in the SLM process: (i) liquid phase sintering (LPS) with full melting of Ni and Fe powders but non-melting of W powders and (ii) melting/solidification with full melting of W powders. Moreover, with increasing laser energy, a transition trend of forming mechanism from LPS to full melting/solidification can be observed.

Keywords microstructure, process window, selective laser melting, W-Ni-Fe alloy

1. Introduction

Selective laser melting (SLM) is a laser based rapid manufacturing technology that builds metal parts layer-by-layer using metal powders and a computer controlled laser (Ref 1, 2). A component's computer aided design (CAD) model is sliced into thin layers mathematically. After consolidation of one powder layer, a fresh layer of powder is deposited and the laser melting process is repeated until a 3D part is completed. Due to its flexibility in feedstock, the SLM technology enables the fabrication of complex final metal components that cannot be manufactured by other conventional methods (Ref 3).

Although SLM holds great potential in fabrication of complex metallic components, it is still in the stage of development. Until now, much previous literature has been issued on the scope of SLM. The topic of SLM mainly dwells on feasible materials and corresponding forming mechanisms. For instance, the fabricating of titanium (Ref 4, 5), iron-base alloys (Ref 6-11), nickel-base alloys (Ref 12-14), copper-base alloys (Ref 15-18), titanium-base alloys (Ref 19, 20), and metal matrix composites (Ref 21, 22) via laser direct manufacturing has been investigated. However, little work has been reported on the investigation into manufacturing complex W-Ni-Fe parts by SLM. W-Ni-Fe metal composites are important materials since they exhibit high density, comprehensive mechanical properties, and good corrosion resistance, leading to many practical applications (Ref 23). Nevertheless, owing to the high melting point of tungsten (3420 °C) (Ref 24), these alloys are usually fabricated through conventional powder metallurgy (PM) techniques (Ref 25), which need expensive and dedicated tools. PM techniques are capable of high efficiencies and dense structures, but they are not suitable for producing complex shapes, which the SLM method is.

As demonstrated in the present article, there are many practical applications in rapid manufacturing of W-Ni-Fe parts by SLM technology. The SLM-fabricated W-Ni-Fe parts can be used in many engineering fields, such as kinetic energy penetrators, radiation shielding, mass balance for aerospace, vibrating masses for cell phones, etc. The advantages of SLM can be obviously realized when W-Ni-Fe components require a complex shaped final configuration, where SLM as a flexible net-shape route can meet this demand with strong advantages of random geometry design and rapid manufacturing.

When the W-Ni-Fe parts are manufactured by SLM instead of conventional PM, the change is not only in aspect of a simple forming pattern variation, but also a complex metallurgical process variation, since the SLM process involves multiple modes of heat, mass, and momentum transfer (Ref 6, 26). In this article, we studied the fabrication of the W-Ni-Fe alloy by SLM technology with a fiber laser as an energy input in detail. The processing behavior, phase transformation, microstructure evolution, and densification behavior in the process of laser irradiation were also addressed.

2. Experimental Procedure

2.1 Powder Materials

W powders (99% purity), carbonyl iron powders (99% purity), and carbonyl nickel powder (99% purity) were used in this experiment (supplier: Dyna-Vitaty Science and Technology Development Company, Beijing). The three kinds of powder were blended according to W:Ni:Fe weight ratio 90:7:3.

Danqing Zhang, Qizhou Cai, and **Ruidi Li**, State Key Laboratory of Material Processing and Die and Mould Technology, Huazhong University of Science and Technology, Wuhan 430074, PR China; **Jinhui Liu**, Heilongjiang Institute of Science and Technology, Harbin 150027, PR China and State Key Laboratory of Powder Metallurgy, Central South University, Changsha 410083, PR China. Contact e-mails: caiqizhou@mail.hust.edu.cn, zdqhust@gmail.com.

A mixing experiment was performed in a stirring mixer for 8 h so that homogeneous SLM composites materials were prepared with argon gas as protection gas. The morphology of the raw powder was examined by a Quanta 200 scanning electron microscope (SEM).

2.2 Laser Processing

The typical process of SLM of W-Ni-Fe alloys has three main procedures: (i) a thin layer of metal powder is deposited by the powder feeder; (ii) the powder is melted by the laser with high energy input; (iii) the bed drops down a layer thickness; with the repeat of above actions the full component could be fabricated. The system was equipped with a 100 W CW/modulated fiber laser with a wavelength of 1095 nm and a rated focal spot diameter of 30 μm. During the SLM process, the chamber is vacuumed then filled with argon gas, so the oxygen volume could decrease to about 10-20 ppm. The various scopes of SLM processing parameters were listed as follows: laser power of 10-100 W, scan speed of 10-180 mm/s, scan interval of 0.05-0.15 mm, and layer thickness of 0.05-0.1 mm. Through the above process procedures, W-Ni-Fe components were successfully manufactured (Fig. 1).

2.3 Characterization

The Vicker's Hardness (HV) of specimens was measured with a HV-1000 micro hardness tester (supplier: Microcre Light-machine Technology Company). Samples for metallographic examination were prepared according to the standard procedures, and etched with a mixture of $NH_3 \cdot H_2O$ (10%, 10 mL), H_2O_2 (10%, 10 mL), and distilled water (20 mL) for about 20 s. The surface morphologies and microstructure of samples were examined with SEM in both secondary electron (SE) and back-scattered electron (BSE) modes. For chemical composition analysis, energy dispersive x-ray spectrometer (EDX) analysis was used. Phase identification was performed with an X' Pert PRO x-ray diffraction (XRD) analyser.

3. Results and Discussion

The investigated mixed powders in the SLM process were blended with W powder, Ni powder, and Fe powder. Figure 2 shows the morphologies of the raw powders. The W powder, acting as the structural metal, shows a polygonal shape with particle size distribution of 1-5 μm (Fig. 2a). Such fine polygonal particles in powder system can promote a higher coordination number which accelerate densification behavior during laser irradiation process. The carbonyl Ni powder with an average particle size of 2.3 μm (Fig. 2b) and carbonyl Fe powder with a mean particle size of 3 μm (Fig. 2c), act as the binders, also exhibit small particle sizes. These relatively fine particles with larger specific surface area can facilitate the absorption of laser energy input and accordingly increase the particle temperature and sintering characteristic (Ref 7). Figure 2(d) shows that the composite powders were mixed uniformly. The homogeneity of a powder mixture is significant to promote the ratio of laser absorption and improve its flowing behavior during SLM, which may ultimately accelerate liquid wetting properties and particle rearrangement (Ref 27). Furthermore this bimodal mixture, mixed by the fine powders with different particle sizes, can increase the loose packing density which is beneficial to SLM technology (Ref 28).

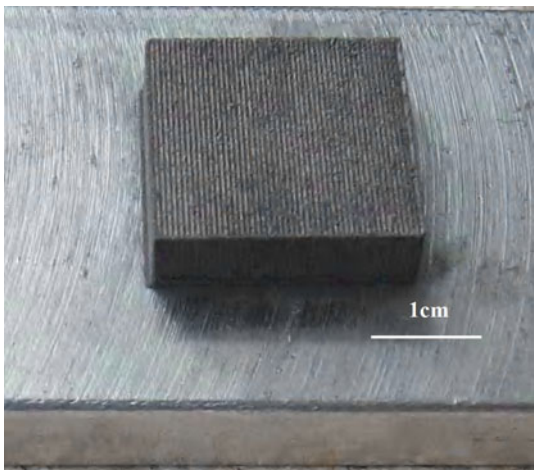

Fig. 1 SLM-fabricated W-Ni-Fe sample

In this study, a series of single layer were produced by a wide range of laser powers and scan speeds, for the purpose of obtaining well bonded layers, since SLM is a multi-layered technique in forming a 3D entity. Figure 3 shows the process windows to describe the melting states of the single layer forming.

- *Moderate melting*: At a high laser power and a low scan speed, the input laser energy was adequate to produce uninterrupted molten tracks, resulting in a relative dense surface without obvious cracks and spheres (Fig. 4a). This compact surface is preferred in SLM process.
- *Spheroidisation phenomenon*: Using a high laser power combined with a high scan speed, liquid scan tracks with long, thin, and cylindrical shape occurred, which were separated into a series of balls due to reduction of surface energy (Fig. 4b). This "balling" effect is detrimental to interlay bonding and causes defects such as curling deformation and poor densification in fabrication of a 3D component.
- *Slight melting*: At a moderate laser power and a low scan speed, the delivered laser energy was insufficient to fully melt the Ni and Fe powder, thereby leaving some residual powders (Fig. 4c).
- *No melting*: At a lower laser power, the laser energy was inadequate to melt the Ni and Fe powders, resulting in an unbonded laser irradiated zone. Thus, multi-layer forming could not have been completed.

The process windows are established according to different laser melting states. The laser parameters depict a similarity of laser melting states in each process window. Then the boundaries were defined proximately. Typical surface morphologies of single layer formation in the corresponding processing windows are illustrated in Fig. 4. As shown in Fig. 3, it can be seen that the feasible process zone is in a limited range. Therefore, these process windows could provide an instruction in choosing proper laser parameters for subsequent layer-by-layer formation.

Figure 5 depicts the typical XRD spectrum of the raw W-Ni-Fe powder blend (a) and the laser fabricated alloys (b) with processing parameters of laser power of 100 W, scan speed of 20 mm/s, scan interval of 0.1 mm, and layer thickness

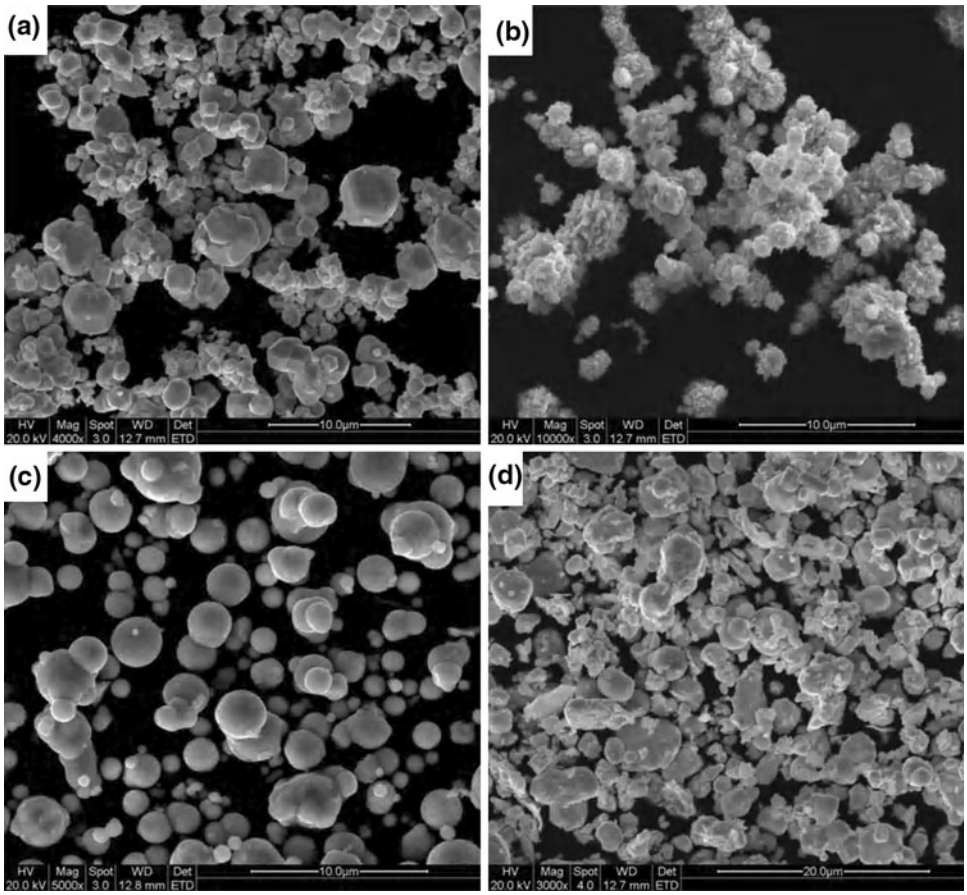

Fig. 2 Characteristic morphologies of raw metal powder in SEM image: (a) tungsten powder, (b) nickel powder, (c) iron powder, and (d) powder mixture

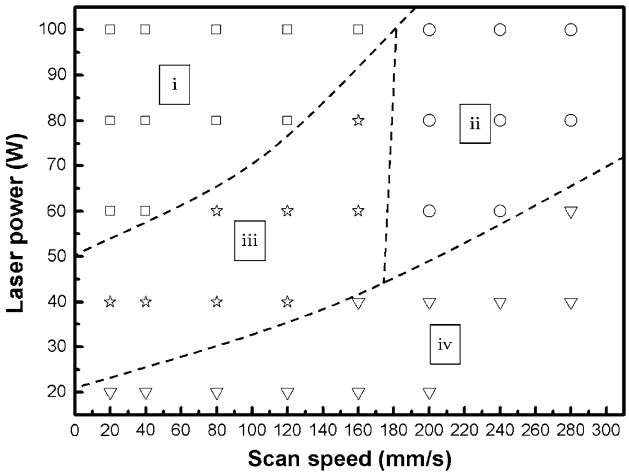

Fig. 3 Process windows for melting states of W-Ni-Fe powder system over a wide range of laser powers and scan speeds

of 0.05 mm. The raw powder blend consisted of a main metal W and a small amount of metal Ni. The diffraction peaks of the metal Fe did not appear because of its minor volume fraction. After the laser scanned with a high energy density, the Ni peaks disappeared and a Ni-Fe solid solution phase came into being.

Figure 6 shows the typical microstructure of the SLM sample at scan speed of 50 mm/s, laser power of 100 W, scan interval of 0.1 mm, and layer thickness of 0.05 mm. As shown in Fig. 6(a), the sample contains two kinds of morphological zone. One is the cellular morphological zone; the other is the dendrite morphological zone.

In the zone with cellular morphology, the W particles were not melted and uniformly dispersed while the Ni and Fe particles were fully melted and bonded un-melted W particles. Therefore, in this zone, the maximum temperature exceeded the melting point of Ni (1452 °C) and Fe (1539 °C) (Ref 29), but was lower than the melting point of W (3420 °C). Consequently, liquid phase sintering (LPS) with complete melting of the Ni and Fe but non-melting of the W particles proves to be a reasonable laser forming mechanism. In this process, Ni-Fe liquid phase can bind W particles rapidly due to the capillary forces applied to the liquid. Meanwhile, W particles rearrangement and grain shape accommodation occurred in this LPS process and it contributed to the densification. In fact, the W powders acted as structural metal in the SLM process, while the Ni and Fe powders acted as the binder, owing to the higher melting point of W than Ni and Fe. For this reason, this LPS process of SLM W-Ni-Fe powders, to a certain degree, represents a similar densification principle to conventional PM. However, it should be noted that there are two different aspects in LPS from conventional PM technique. On one hand, in this special LPS process of SLM, particle rearrangement

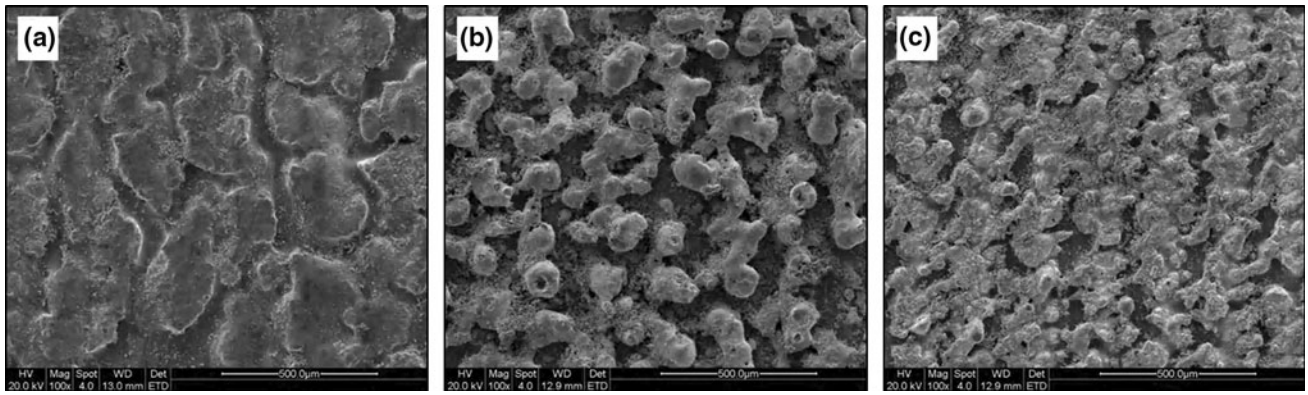

Fig. 4 SEM images showing surface morphologies of single layer forming within different zones in Fig. 3 (the scan intervals were fixed at 0.1 mm): (a) p = 100 W, v = 10 mm/s; (b) p = 100 W, v = 300 mm/s; and (c) p = 60 W, v = 80 mm/s

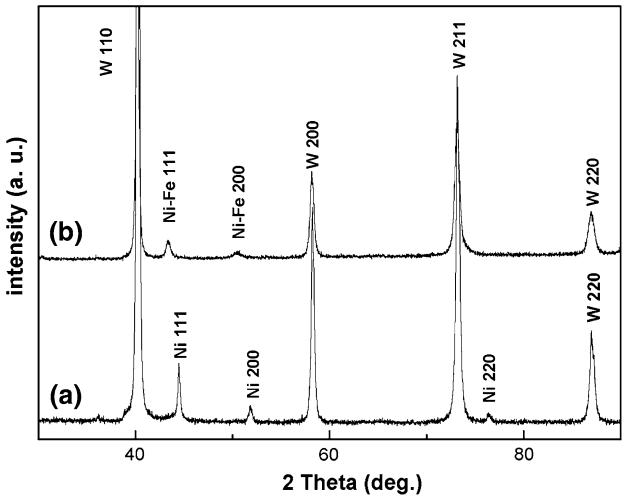

Fig. 5 XRD spectra of the staring W-Ni-Fe powder blend (a) and the laser fabricated sample (b)

occurred for several times, owing to the overlaps of laser scanned lines in each fabrication layer. On the other hand, the sintering time in SLM process is extremely short. After the Ni-Fe liquid phase completely cooled down, no further stage of solid state sintering took place.

Interestingly, the results, shown in Fig. 6(a), reveal a progressive transition from a cellular morphology to dendrite morphology in different zones. In addition, the EDX results reveal that all white color phase is W, while the black color phase is Ni and Fe (Fig. 6b, 7). The hardness of white color phase is approximately 700 HV and the black color phase is approximately 100 HV. This indicates that the forming mechanisms of the laser produced W-Ni-Fe alloys are dissimilar in different microscopic zones. In fact, during SLM processing, the duration of the laser beam on any powder particle depends on both spot size and scan speed, and is typically between 0.5 and 25 ms (Ref 30). In such a short period of time, the high laser power density can easily lead to a large temperature gradient between the center and edge of the molten pool. Thus, a progressive transition from the dendrite morphology to the cellular morphology occurred along a temperature gradient. Therefore, different temperature ranges can yield dissimilar microstructure features and accordingly dissimilar laser forming mechanisms.

The dendrite morphology zone shows a progressive transition from the cellular morphology to the dendrite morphology in different zones. The EDX results reveal that all white color phase is W, while the black color phase is Ni and Fe (see Fig. 6b, 7). In this zone, the laser irradiation with high energy density enabled the temperature to rise above the W melting point, and consequently the W particles were melted during SLM process. For this reason, full melting/solidification approach acts as a feasible mechanism in this zone. It can also be seen that the dendrites grew directionally along a certain preferred but not invariable orientations. Because of a considerable temperature gradient in the molten pool, the dendrites grew directionally along the thermal flow direction. In addition, the preferred orientation of the grains indicates notable effect on the direction of the growing dendrites. The variation of thermal flow direction occurred with the solid/liquid interface advancing on account of the multiple modes effects induced by the laser scan (Ref 16). Hence, the W dendrites may adjust their growing direction in response to thermal flow direction. Moreover, it should be pointed out that the vaporization of partial Ni-Fe liquid phase may take place in light of the high temperature being in exceed of Ni and Fe vaporizing points. Gu and Shen have reported laser sintered W-Cu by a CO_2 laser beam (Ref 31). Their investigations have shown that on laser sintering, an LPS is the forming mechanism with a sintering pool containing both liquid (Cu) and solid (W) phase. However, under the SLM of W-Ni-Fe used in the present study, the W particles are partially melted, forming a dendrite feature. The different forming mechanisms in laser fabricated W-base alloys can be explained by two main reasons. First, in the present study of SLM W-Ni-Fe alloy, the fiber laser was used, which operates at lower wavelengths and a smaller spot size compared with CO_2 laser. It is known that the absorption ratio of metals to fiber laser beam is higher than that to CO_2 laser beam (Ref 32). Thus, the effective laser energy with fiber laser is higher than that with CO_2 laser accordingly resulting in a higher temperature in the melt pool. Second, the higher thermal conductivity of metal Cu than Ni and Fe induced a more rapid heat dissipation in W-Cu alloy than W-Ni-Fe alloy, thereby a lower molten pool temperature below melting point of W particles.

In order to explore the influence of higher laser energy on the microstructure evolution, the scan speed, and scan interval

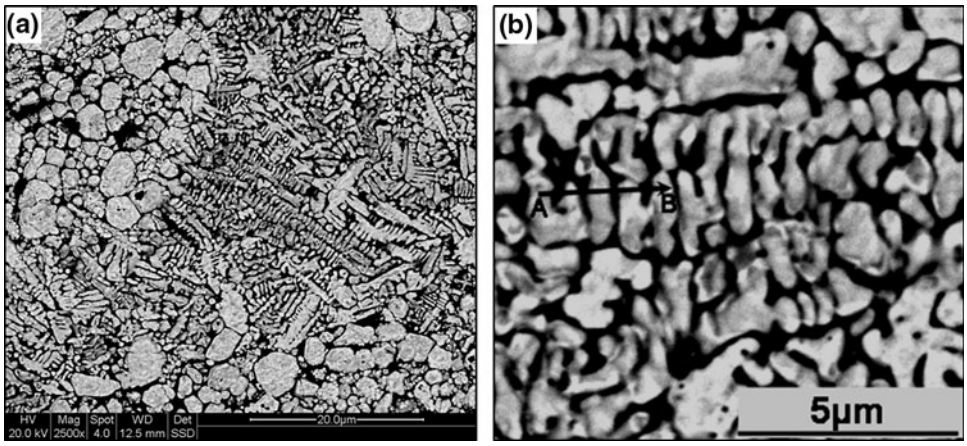

Fig. 6 BSE images showing microstructures of a laser fabricated sample at scan speed of 50 mm/s, laser power of 100 W, scan interval of 0.1 mm and layer thickness of 0.05 mm with different magnifications: (a) 2500× and (b) 10,000×

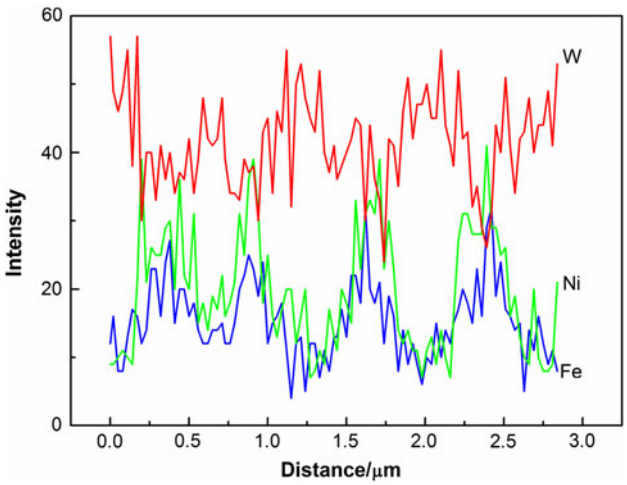

Fig. 7 Distributions of W, Ni, and Fe elements shown by EDX trace along AB line in Fig. 6b

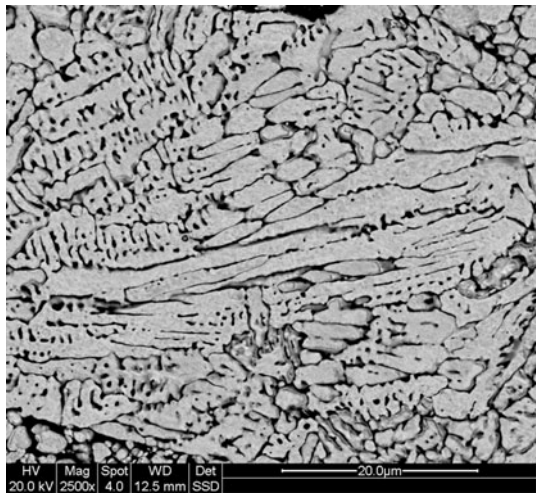

Fig. 8 BSE images showing microstructures of a laser fabricated sample at scan speed of 20 mm/s, laser power of 100 W, scan interval of 0.05 mm, and layer thickness of 0.05 mm

were decreased to 20 mm/s, 0.05 mm, respectively, with the other parameters were fixed (laser power of 100 W and layer thickness of 0.05 mm). The microstructure of fabricated part is shown in Fig. 8. It can be found that this microstructure presents nearly full dendrite feature, which is obviously different from the microstructure in Fig. 6(a). Moreover, the dendrite grains coarsened with decreasing scan speed compared with Fig. 6(a). The differences of microstructure with different scan speeds and scan intervals can be explained by comparing the laser energy induced in the powder bed. It is known that the energy input is inversely proportional to the scan speed and scan interval, in other words, with decreasing the scan speed and scan interval, the laser energy input increases. Therefore, the temperature field increases and heat effect ranges enlarge, causing most W particles melted. Moreover, the decreased scan speed results in a longer duration of the laser beam on the powder bed and thus it accelerates grains growth. In all, the microstructure of laser fabricated W-Ni-Fe parts with partial or full melting of W particles, to a great degree, is evidently different from microstructure obtained by PM method.

4. Conclusions

The SLM method was innovatively used to manufacture the W-Ni-Fe parts in the present study. Based on the experiments conducted, conclusions can be obtained as follows:

(1) The W-Ni-Fe mixed powders prepared in this work can be used to manufacture parts with complex shapes needed in practical engineering, showing very little dimensional deformation and "balling" phenomena.
(2) A workable process map is developed by investigating the influence of laser powers and scan speeds on the melting surface state in single layer forming. This process map can provide an instruction in selection of proper parameters.
(3) There are two coexisting forming mechanisms in the SLM process: (i) LPS with full melting of Ni and Fe powders but non-melting of W powders and (ii) melting/solidification with full melting of W powders. Moreover,

with increasing laser energy, a transition trend of forming mechanism from LPS to full melting/solidification can be observed.

(4) With increasing laser energy, the transition trend from LPS to full melting/solidification became remarkable. The microstructure of W-Ni-Fe alloy mainly consists of dendrite morphology.

Acknowledgments

The authors would like to thank the Open fund of State Key Laboratory of Powder Metallurgy of Central South University of China (2008112022). The authors also thank the Analytic and Testing Centre of Huazhong University of Science and Technology for their assistance.

References

1. F. Abe, K. Osakada, M. Shiomi, K. Uematsu, and M. Matsumoto, The Manufacturing of Hard Tools from Metallic Powders by Selective Laser Melting, *J. Mater. Process. Technol.*, 2001, **111**(1–3), p 210–213
2. E.C. Santos, M. Shiomi, K. Osakada, and T. Laoui, Rapid Manufacturing of Metal Components by Laser Forming, *Int. J. Mach. Tools Manuf.*, 2006, **46**(12–13), p 1459–1468
3. A. Simchi, F. Petzoldt, and H. Pohl, On the Development of Direct Metal Laser Sintering for Rapid Tooling, *J. Mater. Process. Technol.*, 2003, **141**(3), p 319–328
4. X. Wu and J. Mei, Near Net Shape Manufacturing of Components Using Direct Laser Fabrication Technology, *J. Mater. Process. Technol.*, 2003, **135**(2–3), p 266–270
5. P. Fischer, V. Romano, H.P. Weber, N.P. Karapatis, E. Boillat, and R. Glardon, Sintering of Commercially Pure Titanium Powder with a Nd: YAG Laser Source, *Acta Mater.*, 2003, **51**(6), p 1651–1662
6. A. Simchi and H. Pohl, Direct Laser Sintering of Iron-Graphite Powder Mixture, *Mater. Sci. Eng. A Struct. Mater. Prop. Microstruct. Process.*, 2004, **383**(2), p 191–200
7. A. Simchi, Direct Laser Sintering of Metal Powders: Mechanism, Kinetics and Microstructural Features, *Mater. Sci. Eng. A Struct. Mater. Prop. Microstruct. Process.*, 2006, **428**(1–2), p 148–158
8. J.P. Kruth, L. Froyen, J. Van Vaerenbergh, P. Mercelis, M. Rombouts, and B. Lauwers, Selective Laser Melting of Iron-Based Powder, *J. Mater. Process. Technol.*, 2004, **149**(1–3), p 616–622
9. Y. Wang, J. Bergstrom, and C. Burman, Characterization of an Iron-Based Laser Sintered Material, *J. Mater. Process. Technol.*, 2006, **172**(1), p 77–87
10. A. Simchi and H. Pohl, Effects of Laser Sintering Processing Parameters on the Microstructure and Densification of Iron Powder, *Mater. Sci. Eng. A Struct. Mater. Prop. Microstruct. Process.*, 2003, **359**(1–2), p 119–128
11. M.L. Sun, L. Lu, and J.Y.H. Fuh, Microstructure and Properties of Fe-Base Alloy Fabricated Using Selective Laser Melting, *2nd International Symposium on Laser Precision Microfabrication*, I. Miyamoto, Y.F. Lu, K. Sugioka, and J.J. Dubowski, Ed., Singapore, 2001, p 139–142
12. K.A. Mumtaz, P. Erasenthiran, and N. Hopkinson, High Density Selective Laser Melting of Waspaloy (R), *J. Mater. Process. Technol.*, 2008, **195**(1–3), p 77–87
13. C.P. Paul, P. Ganesh, S.K. Mishra, P. Bhargava, J. Negi, and A.K. Nath, Investigating Laser Rapid Manufacturing for Inconel-625 Components, *Opt. Laser Technol.*, 2007, **39**(4), p 800–805
14. K. Mumtaz and N. Hopkinson, Top Surface and Side Roughness of Inconel 625 Parts Processed Using Selective Laser Melting, *Rapid Prototyping J.*, 2009, **15**(2), p 96–103
15. H.H. Zhu, L. Lu, and J.Y.H. Fuh, Development and Characterisation of Direct Laser Sintering Cu-Based Metal Powder, *J. Mater. Process. Technol.*, 2003, **140**, p 314–317
16. D.D. Gu and Y.F. Shen, Development and Characterisation of Direct Laser Sintering Multicomponent Cu Based Metal Powder, *Powder Metall.*, 2006, **49**(3), p 258–264
17. S.R. Pogson, P. Fox, C.J. Sutcliffe, and W. O'Neill, The Production of Copper Parts Using DMLR, *Rapid Prototyping J.*, 2003, **9**(5), p 334–343
18. W.H. Wu, Y.Q. Yang, and Y.L. Huang, Direct Manufacturing of Cu-Based Alloy Parts by Selective Laser Melting, *Chin. Opt. Lett.*, 2007, **5**(1), p 37–40
19. D.A. Hollander, M. von Walter, T. Wirtz, R. Sellei, B. Schmidt-Rohlfing, O. Paar, and H.J. Erli, Structural, Mechanical and In Vitro Characterization of Individually Structured Ti-6Al-4V Produced by Direct Laser Forming, *Biomaterials*, 2006, **27**(7), p 955–963
20. K. Osakada and M. Shiomi, Flexible Manufacturing of Metallic Products by Selective Laser Melting of Powder, *Int. J. Mach. Tools Manuf.*, 2006, **46**(11), p 1188–1193
21. D.D. Gu and Y.F. Shen, WC-Co Particulate Reinforcing Cu Matrix Composites Produced by Direct Laser Sintering, *Mater. Lett.*, 2006, **60**(29–30), p 3664–3668
22. D.D. Gu, Z.Y. Wang, Y.F. Shen, Q. Li, and Y.F. Li, In Situ TiC Particle Reinforced Ti-Al Matrix Composites: Powder Preparation by Mechanical Alloying and Selective Laser Melting Behavior, *Appl. Surf. Sci.*, 2009, **255**(22), p 9230–9240
23. H.H. Soon and H.J. Ryu, Combination of Mechanical Alloying and Two-Stage Sintering of a 93W-5.6Ni-1.4Fe Tungsten Heavy Alloy, *Mater. Sci. Eng. A Struct. Mater. Prop. Microstruct. Process.*, 2003, **344**(1–2), p 253–260
24. A. Upadhyaya, S.K. Tiwari, and P. Mishra, Microwave Sintering of W-Ni-Fe Alloy, *Scr. Mater.*, 2007, **56**(1), p 5–8
25. J. Shen, L. Campbell, P. Suri, and R.M. German, Quantitative Microstructure Analysis of Tungsten Heavy Alloys (W-Ni-Cu) During Initial Stage Liquid Phase Sintering, *Int. J. Refract. Met. Hard Mater.*, 2005, **23**, p 99–108
26. S. Das, Physical Aspects of Processing Control in Selective Laser Sintering of Metals, *Adv. Eng. Mater.*, 2003, **5**, p 701–711
27. A. Simchi, F. Petzoldt, and H. Pohl, Direct Metal Laser Sintering: Material Considerations and Mechanisms of Particle Bonding, *Int. J. Powder Metall.*, 2001, **37**(2), p 49–61
28. P. Wang, *Powder Metallurgy*, Beijing Technology University, Metallurgy Industry Publishing Company, Beijing, 2000 (in Chinese)
29. T.B. Massalski, *Binary Alloy Phase*, ASM International, Material Park, OH, 1996
30. D.D. Gu, Y.F. Shen, J.L. Yang, and Y. Wang, Effects of Processing Parameters on Direct Laser Sintering of Multicomponent Cu Based Metal Powder, *Mater. Sci. Technol.*, 2006, **22**(12), p 1449–1455
31. D.D. Gu, Y.F. Shen, and X.J. Wu, Formation of a Novel W-Rim/Cu-Core Structure During Direct Laser Sintering of W-Cu Composite System, *Mater. Lett.*, 2008, **62**(12–13), p 1765–1768
32. K. Lai, Y. Yang, and L. Zhang, Fiber Laser and its Applications in Rapid Prototyping of Selective Laser Melting, *Laser Optoelectron. Prog.*, 2006, **43**, p 32–36 (in Chinese)